Research Article Vol. 6, No. 1 / January 2019 / Optica 45

Kramers–Kronig holographic imaging for high-space-bandwidth product

YoonSeok Baek,[1,2] KyeoReh Lee,[1,2] Seungwoo Shin,[1,2] and YongKeun Park[1,2,3,*]

[1]Department of Physics, Korea Advanced Institute of Science and Technology (KAIST), Daejeon 34141, South Korea
[2]KAIST Institute for Health Science and Technology, KAIST, Daejeon 34141, South Korea
[3]Tomocube, Inc., 48, Yuseong-daero 1184beon-gil, Yuseong-Gu, Daejeon 34051, South Korea
*Corresponding author: yk.park@kaist.ac.kr

Received 9 October 2018; revised 28 November 2018; accepted 4 December 2018 (Doc. ID 347840); published 7 January 2019

Modern optical imaging possesses a huge information capacity whose corresponding space-bandwidth product (SBP) reaches tens of megapixels. However, despite the advances in optical and electronic devices, the SBP of an optical microscope is greatly limited, resulting in a reduced field of view or resolution of an image. In this paper, we exploit the Kramers–Kronig relations in digital holography to achieve high SBP imaging, demonstrating a complex amplitude image that can surpass the SBP of a bright-field image. The capability of the proposed method is demonstrated by imaging static samples and biological tissues. We successfully measure a 4.2-megapixel complex amplitude image whose bright-field counterpart exhibits 16.7 megapixels.

https://doi.org/10.1364/OPTICA.6.000045

1. INTRODUCTION

The space-bandwidth product (SBP) [1] of an imaging system describes the amount of information generated by the system. In microscopy, the SBP is defined by the product of the area of the field of view (FoV) and the area of the spatial frequency band of an image. Although the SBP of a modern microscope reaches up to tens of megapixels, the practical SBP is limited to only a few megapixels. This is because the number of pixels in a commercially available image sensor is much lower than the SBP the optical microscope can provide. Thus, the majority of optical information remains undetected, limiting the advance of microscopy for large-scale high-throughput imaging, which is essential for digital histology [2], drug discovery [3], and cell biology [4].

Recently, several methods have attempted to overcome the limitations of the SBP. Based on phase-retrieval algorithms, iterative methods such as Fourier ptychography [5,6], out-of-focus imaging [7], and pixel super-resolution [8] offer enhanced SBPs in imaging that exceed SBPs of detectors. However, there are certain prerequisites if these methods are to obtain correct images; Fourier ptychography requires images to have data redundancy in the frequency domain, out-of-focus imaging needs a weakly scattering sample and images at different axial positions, and the pixel super-resolution method requires precisely controlled subpixel shifts between images. Furthermore, since these methods enhance SBPs by combining information from multiple images, they require multiple measurements and have low SBPs per measurement.

An interesting approach related to this issue can be found in radio communication. Single-sideband modulation adopts a complex amplitude signal to reduce signal bandwidth [9], exploiting the fact that the bandwidth of a complex amplitude signal is smaller than that of a real-valued signal. Since the same principle holds in imaging [10], a similar strategy can be considered in optical microscopy; one can measure a complex amplitude image instead of an intensity image to obtain a higher SBP, because the bandwidth of a complex amplitude image is less than that of an intensity image at the same FoV.

Holographic imaging is an effective way to acquire a complex amplitude image with a microscope and to investigate transparent microscopic objects such as cells and tissues [11–13]. In particular, off-axis holography [14,15] enables single-shot measurement of a complex amplitude image. This is achieved with an off-axis interferogram that isolates the complex amplitude image from its twin image, and autocorrelation in the spatial frequency domain. However, as a result, an off-axis interferogram has a broad bandwidth, which is inefficient regarding the SBP of the complex amplitude image.

To improve the SBP of off-axis holographic imaging, various techniques have been suggested. For example, methods utilizing multiplexing [16–18] and aliasing [19] show efficient uses of the finite bandwidth of an image sensor. Alternatively, reductions in the interferogram bandwidth are achieved by subtracting the autocorrelation using multiple interferograms [20,21], or by suppressing it through numerical methods [22,23], speckle [24], a wavelet transform [25], Hilbert transform [26], or an optimization algorithm [27], at the cost of sample constraints. Nonlinear filtering methods based on the Fresnelet transform [28], the cepstrum [29], an iterative algorithm [30], and a local weighted least squares estimation [31] suppress the autocorrelation without

imposing a condition on a sample. However, they require time-consuming iterative processes, *a priori* information about samples, or certain imaging conditions. The Fresnelet method requires a Fresnel hologram and different thresholding of Fresnelet coefficients depending on the sample. The cepstrum method and the iterative algorithm require a strong reference and a complex amplitude image to be confined within a quadrant of the spatial frequency domain. The least squares estimation needs modification in weighting windows and sampling conditions depending on local spatial frequency of an interferogram. Furthermore, none of the previous studies has demonstrated the capability of off-axis holographic imaging to surpass bright-field imaging regarding the SBP.

Here, we propose and experimentally demonstrate a general method for high SBP holographic imaging exploiting the Kramers–Kronig (KK) relations. To retrieve a complex amplitude image, we introduce a complex analytic function whose real part is described by an off-axis interferogram. Then the KK relations recover the complex analytic function, from which the complex amplitude image is retrieved. The proposed method is guaranteed by the analyticity of the complex function that does not impose a constraint on a sample. Importantly, the analyticity holds even when the complex amplitude image is completely overlapped with its autocorrelation in the frequency space of the interferogram. Thus, the proposed method requires a greatly reduced interferogram bandwidth, achieving high SBP imaging beyond what has been demonstrated in conventional off-axis holographic imaging. We demonstrate the capability of the proposed method by imaging various samples, including a resolution target, polystyrene beads, human breast tissue, and mouse brain tissue. Furthermore, by maximizing the capability of the method with anamorphic imaging, we successfully measured a 4.2-megapixel complex amplitude image whose bright-field counterpart exhibits an SBP (16.7 megapixels) greater than the SBP of the detector (12 megapixels).

2. PRINCIPLE

A. Conventional Off-Axis Holographic Imaging

In conventional off-axis holographic imaging, a reference beam $R(\boldsymbol{r})$ interferes with a sample beam $S(\boldsymbol{r})$ with a slight tilt angle θ. The reference beam is a quasi-plane wave with a wavelength of λ, which is expressed as $R(\boldsymbol{r}) = R_0 e^{i2\pi\nu_R\cdot\boldsymbol{r}}$, where ν_R is the spatial frequency vector of $R(\boldsymbol{r})$ with $|\nu_R| = \sin\theta/\lambda$. Then the two beams form an interferogram, $I(\boldsymbol{r}) = |S + R|^2$, whose Fourier transformation can be written as

$$\tilde{I}(\nu) = \tilde{A}(\nu) + \tilde{B}(\nu - \nu_R) + \tilde{B}^*(-\nu - \nu_R), \tag{1}$$

where $\tilde{A}(\nu) = \mathcal{F}[|S|^2 + |R|^2]$, $\tilde{B}(\nu) = \mathcal{F}[R_0 S]$, and $\mathcal{F}$ indicates Fourier transform. In Eq. (1), $\tilde{B}(\nu - \nu_R)$ is centered at ν_R due to the spatial modulation of $R(\boldsymbol{r})$; conventional off-axis interferometry utilizes this translation to isolate $\tilde{B}(\nu - \nu_R)$ from $\tilde{A}(\nu)$.

The signal isolation is achieved by choosing a large ν_R to avoid overlaps among the three terms in Eq. (1). The exact condition for ν_R can be determined by considering the pupil function of an imaging system. For an ideal imaging system having a numerical aperture of an objective lens of $\mathrm{NA}_{\mathrm{obj}}$ and a transverse magnification of M, the pupil function $\tilde{P}(\nu)$ can be expressed as

$$\tilde{P}(\nu) = \begin{cases} 1, & |\nu| \le \mathrm{NA}_{\mathrm{obj}}/\lambda M \\ 0, & |\nu| > \mathrm{NA}_{\mathrm{obj}}/\lambda M \end{cases}. \tag{2}$$

Thus, a sample beam transmitted through the imaging system is band-limited; $\tilde{S}(\nu) = \tilde{P}(\nu)\tilde{S}(\nu)$. Also, $\tilde{B}(\nu)$ becomes band-limited, i.e., $\tilde{B}(\nu) = R_0\tilde{P}(\nu)\tilde{S}(\nu)$. Similarly, $\tilde{A}(\boldsymbol{r})$ is band-limited and has a Fourier transform defined within the autocorrelation of $\tilde{P}(\nu)$, which has a radius of $2\mathrm{NA}_{\mathrm{obj}}/\lambda M$ [32]. Thus, to guarantee no overlap between $\tilde{A}(\boldsymbol{r})$ and $\tilde{B}(\nu - \nu_R)$, ν_R must satisfy

$$|\nu_R| > 3\frac{\mathrm{NA}_{\mathrm{obj}}}{\lambda M}. \tag{3}$$

Under this condition, $\tilde{B}(\nu)$ can be obtained by filtering in the frequency domain, as $\tilde{B}(\nu) = \tilde{I}(\nu + \nu_R)\tilde{P}(\nu)$. The complex amplitude image, $R_0 S$, is then retrieved by the inverse Fourier transformation of $\tilde{B}(\nu)$. Ideally, the condition in Eq. (3) can be met by adequately adjusting θ. However, in practice, this condition is met by reducing the size of a pupil function (either by increasing magnification or decreasing the numerical aperture) due to the limited bandwidth of the detector. As a result, the SBP of a complex amplitude image is greatly limited in the conventional off-axis method.

B. Kramers–Kronig Holographic Imaging

The KK relations connect the imaginary and real parts of a complex function that is analytic in the upper half-plane (UHP) [33,34]. For example, a function $f(\omega)$ that is analytic in the UHP of ω satisfies

$$\mathrm{Re}[f(\omega)] = \frac{1}{\pi}\mathrm{p.v.}\int_{-\infty}^{\infty}\frac{\mathrm{Im}[f(\omega')]}{\omega' - \omega}\mathrm{d}\omega', \tag{4a}$$

$$\mathrm{Im}[f(\omega)] = -\frac{1}{\pi}\mathrm{p.v.}\int_{-\infty}^{\infty}\frac{\mathrm{Re}[f(\omega')]}{\omega' - \omega}\mathrm{d}\omega', \tag{4b}$$

where p.v. indicates Cauchy principal value. First, we propose a function $\chi(\boldsymbol{r}) = \log[1 + \beta(\boldsymbol{r})]$, where $\beta(\boldsymbol{r})$ is the sample-reference ratio; $\beta(\boldsymbol{r}) = S(\boldsymbol{r})/R(\boldsymbol{r})$. From the definition, the real and imaginary parts of $\chi(\boldsymbol{r})$ are expressed as (see Supplement 1)

$$\mathrm{Re}[\chi(\boldsymbol{r})] = \log|1 + \beta(\boldsymbol{r})| = \frac{1}{2}[\log I(\boldsymbol{r}) - \log|R(\boldsymbol{r})|^2], \tag{5a}$$

$$\mathrm{Im}[\chi(\boldsymbol{r})] = \arg[1 + \beta(\boldsymbol{r})]. \tag{5b}$$

Note that the real part can be obtained from the interferogram and the image of the reference beam. The full knowledge of $\chi(\boldsymbol{r})$ gives the complex amplitude of a sample beam as $S(\boldsymbol{r}) = R(\boldsymbol{r})[e^{\chi(\boldsymbol{r})} - 1]$. However, direct access to $\chi(\boldsymbol{r})$ is not possible, since the imaginary part cannot be directly measured. We apply the KK relations to solve this problem. Provided that $\chi(\boldsymbol{r})$ follows the KK relations, its imaginary part can be obtained from its real part through Eq. (4b), which in turn gives the complex amplitude of a sample beam. Therefore, the validity of the KK relations, or equivalently, the analyticity of $\chi(\boldsymbol{r})$, becomes the key condition for successful retrieval of $S(\boldsymbol{r})$ from an interferogram.

The analyticity condition for $\chi(\boldsymbol{r})$ can be found by rewriting it using a Taylor expansion,

$$\chi(\boldsymbol{r}) = \sum_{n=0}^{\infty}\frac{-1^n}{n+1}[\beta(\boldsymbol{r})]^{n+1}, \tag{6}$$

where $|\beta(\boldsymbol{r})| < 1$ is assumed. Since $\chi(\boldsymbol{r})$ is a power series of $\beta(\boldsymbol{r})$, the analyticity of $\chi(\boldsymbol{r})$ is guaranteed by the analyticity

of $\beta(\boldsymbol{r})$ [35,36]. If we assume an off-axis configuration where $R(\boldsymbol{r}) = R_0 e^{-i2\pi\boldsymbol{\nu}_R\cdot\boldsymbol{r}}$, $\beta(\boldsymbol{r})$ is expressed as

$$\beta(\boldsymbol{r}) = \frac{1}{R_0}\int_{-\infty}^{\infty} \tilde{S}(\nu_\parallel, r_\perp)\exp[i2\pi(\nu_\parallel + |\nu_R|)r_\parallel]\mathrm{d}\nu_\parallel, \quad (7)$$

where $\boldsymbol{r} = r_\parallel\hat{\boldsymbol{r}}_\parallel + r_\perp\hat{\boldsymbol{r}}_\perp$ with $\boldsymbol{\nu}_R\cdot\hat{\boldsymbol{r}}_\parallel = |\boldsymbol{\nu}_R|$ and $\boldsymbol{\nu}_R\cdot\hat{\boldsymbol{r}}_\perp = 0$; and $\tilde{S}(\nu_\parallel, r_\perp)$ is the one-dimensional (1D) Fourier transform of $S(\boldsymbol{r})$ with respect to $r_\parallel$. Using the fact a function $f(x)$ is analytic in the UHP of x when its Fourier transform has only positive spatial frequency components [37], $\beta(\boldsymbol{r})$ becomes analytic in the UHP of $r_\parallel$, when $\nu_\parallel + |\nu_R| > 0$ for every $\nu_\parallel$. Exploiting the fact that $S(\boldsymbol{r})$ is band-limited by the pupil function [Eq. (2)], the analyticity condition for $\beta(\boldsymbol{r})$ in the UHP of $r_\parallel$ can be expressed in terms of $|\nu_R|$ as (see Supplement 1 for details about the analyticity and computation of discrete signals)

$$|\nu_R| > \frac{\mathrm{NA}_{\mathrm{obj}}}{\lambda M}. \quad (8)$$

As a result, Eq. (8) guarantees the use of the KK relations between Eqs. (5a) and (5b). In deriving Eq. (8), no condition of the sample beam is required except its band-limitedness. Note that Eq. (8) is a greatly relaxed condition compared to the case of the conventional off-axis method [Eq. (3)]. The proposed method shows a four-fold increase in the SBP compared to the conventional off-axis method with a horizontally/vertically modulated reference beam (or 3.34-fold increase with a diagonally modulated reference; see Supplement 1 for details).

3. EXPERIMENTAL RESULTS

A. Holographic Imaging With and Without a Spectral Overlap

To demonstrate the capability of the proposed method, various samples are imaged, under the condition where $\tilde{A}(\nu)$ and $\tilde{B}(\nu - \nu_R)$ severely overlap in the frequency space; $|\nu_R| = \mathrm{NA}_{\mathrm{obj}}/\lambda M + \varepsilon$ with $\varepsilon > 0$. Interferograms of a 1951 United States Air force (USAF) resolution target (#59-153, Edmund Optics, Barrington, New Jersey, USA) and a 10-μm-diameter polystyrene bead (72986, Sigma-Aldrich, Missouri, USA) are imaged. The experimental setup is shown in Fig. S2. Polystyrene beads are immersed in an index-matching oil with a refractive index of 1.56. Next, complex amplitudes are reconstructed by the proposed method and by the conventional off-axis method, respectively. For comparison, an identical interferogram per sample is used for the two methods. To remove the complex amplitude of illumination, each complex amplitude image of a sample is divided with that measured in the absence of a sample throughout the experiment.

The experimental results are shown in Fig. 1. In the proposed method, the USAF resolution target shows uniform amplitudes and phases at the position of patterns [Figs. 1(a) and 1(b)]. The result of the polystyrene bead shows uniform amplitude and a spherical phase distribution that are consistent with the known shape of the sample [Figs. 1(c) and 1(d)]. The polystyrene bead has a refractive index of 1.575 (at $\lambda = 632.8$ nm), resulting in a phase delay of 2.73 rad, which is consistent with the result [see inset in Fig. 1(d)].

However, in the conventional method, the amplitude and phase of both samples are severely distorted [Figs. 1(e)–1(h)]. The USAF resolution target exhibits stronger noise than for the case of the polystyrene bead, because of the broad spectrum of $\tilde{A}(\nu)$. This is expected from an off-axis interferogram whose fringe pattern has low spatial frequency [Fig. 1(i)]. Due to weak spatial modulation, $\tilde{A}(\nu)$ and $\tilde{B}(\nu - \nu_R)$ are severely overlapped [Fig. 1(j)]. In such a condition, only the analyticity in Eq. (8) is satisfied, not the separation condition in Eq. (3). Thus, the proposed method can reconstruct correct complex amplitude images, while the conventional off-axis method cannot.

To investigate the validity of the proposed method in a conventional condition, the two methods are compared when $\tilde{A}(\nu)$ and $\tilde{B}(\nu - \nu_R)$ are separated in the frequency space;

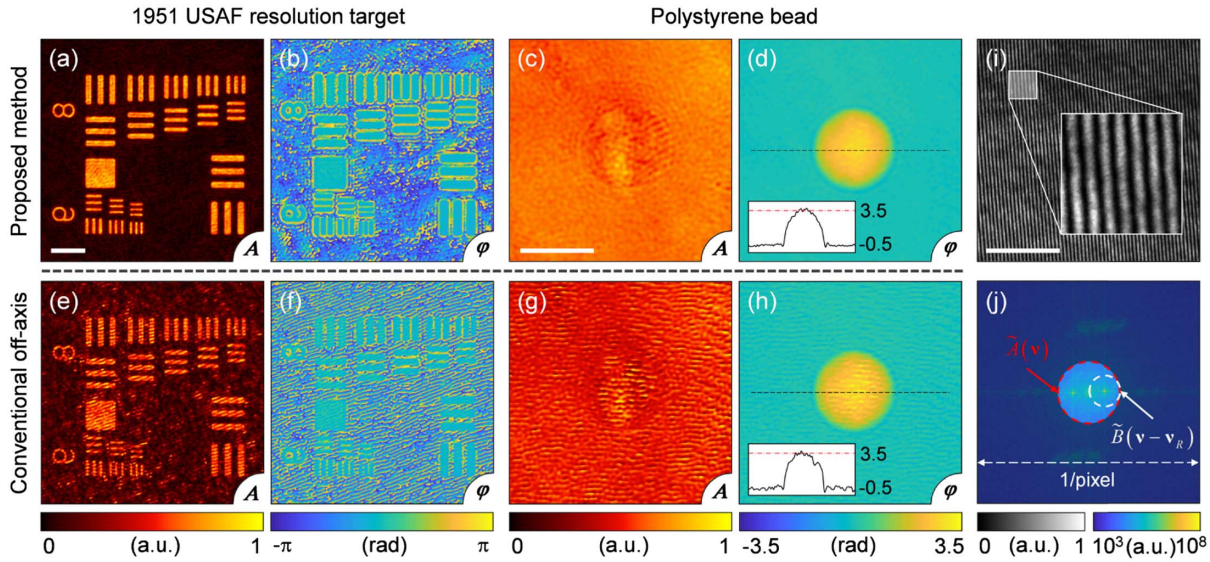

Fig. 1. Experimental demonstration with a spectral overlap. (a)–(d). Experimental results using the proposed method showing a USAF 1951 resolution target (a) and (b), and a 10-μm-diameter polystyrene bead (c) and (d). (e)–(h) Experimental results using a conventional off-axis method showing the resolution target (e) and (f), and the polystyrene bead (g) and (h). (i) Interferogram in the experimental condition. (j) Fourier transform of (i). (Insets) Line profiles of (d) and (h). The red dashed lines correspond to a phase value of 2.73 rad. Scale bars indicate 10 μm.

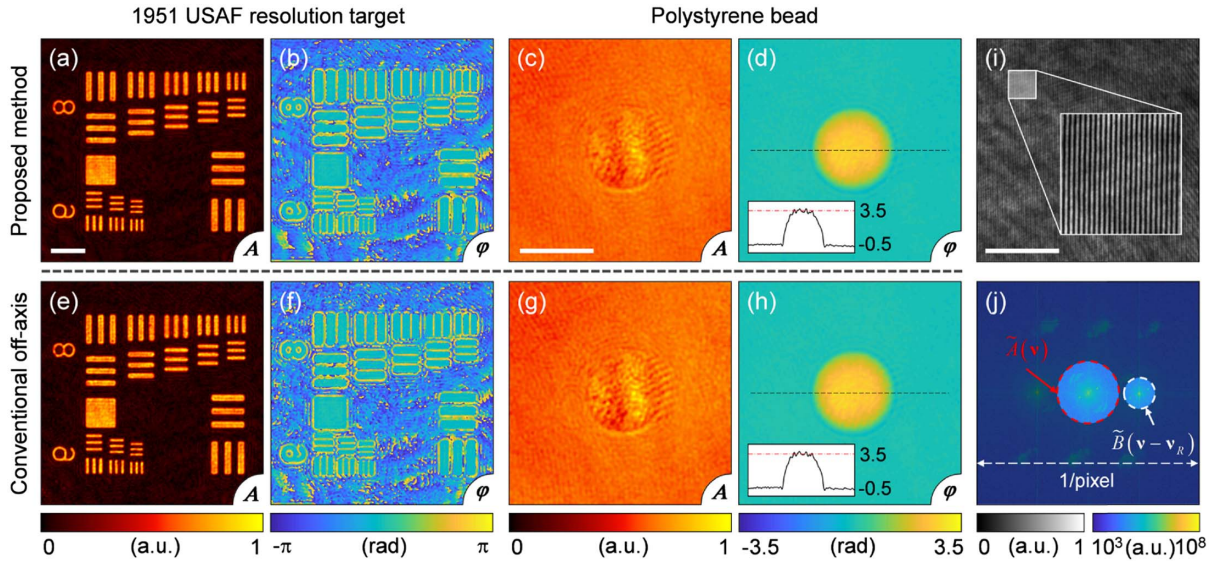

Fig. 2. Experimental demonstration without a spectral overlap. (a)–(d) Experimental results using the proposed method showing a 1951 USAF resolution target (a) and (b), and a 10-μm-diameter polystyrene bead (c) and (d). (e)–(h) Experimental results using a conventional off-axis method showing the resolution target (e) and (f), and the polystyrene bead (g and h). (i) Interferogram in the experimental condition. (j) Fourier transform of (i). (Insets) Line profiles of (d) and (h). The red dashed lines correspond to a phase value of 2.73 rad. Scale bars indicate 10 μm.

$|\nu_R| > 3NA_{\text{obj}}/\lambda M$. Again, the USAF resolution target and a 10-μm-diameter polystyrene bead are used for imaging. The experimental results of the two different methods are shown in Fig. 2. The upper row corresponds to the result of the proposed method [Figs. 2(a)–2(d)], and the bottom row corresponds to the result of the conventional off-axis method [Figs. 2(e)–2(h)]. Both methods show clear holographic images of the USAF resolution target and polystyrene bead. Again, the measured phase value of the polystyrene bead agrees with the expected value of 2.73 rad [see insets in Figs. 2(d) and 2(h)]. More importantly, the results of the two different methods agree with each other. It confirms that the proposed method reconstructs identical information with the conventional off-axis field retrieval method. In this case, the off-axis interferogram has a fringe pattern with high spatial frequency [Fig. 2(i)]. The strong spatial modulation of the reference beam separates $\tilde{B}(\nu - \nu_R)$ from $\tilde{A}(\nu)$ [Fig. 2(j)]. Consequently both the separation condition in Eq. (3) and the analyticity condition in Eq. (8) are satisfied.

B. Wide Field of View Imaging

The biggest advantage of the proposed method is the enhancement in the SBP. Due to the reduced bandwidth of an interferogram, a large amount of information can be measured with a detector having a finite bandwidth and a fixed number of pixels. As an experimental demonstration, wide FoV imaging is conducted with human breast tissue. The tissue is prepared with the standard procedure of formalin fixation and paraffin embedding. For imaging, an objective lens with an NA of 0.4 is adopted (UPLSAPO 10 × 2, Olympus, Tokyo, Japan). The total magnification of the setup is kept at 10, identical to the magnification of the objective lens.

The measured quantitative phase image is shown in Fig. 3(a). The interferogram is imaged when $\tilde{A}(\nu)$ and $\tilde{B}(\nu - \nu_R)$ are completely overlapped [Fig. 3(b)]. The FoV of the image is 1.32 × 0.88 mm with a diffraction-limited size of 0.96 μm. Insets (i, ii) clearly show fine structures of the tissue. The SBP of the complex amplitude image is 1.46 megapixels [the area of the FoV, 1.16 mm^2, multiplied by the area of spatial frequency band, $\pi(\text{NA}/\lambda)^2$]. Figure 3(b) shows the Fourier spectrum of the measured off-axis interferogram. The conventional off-axis method cannot be adopted in this condition, because the diameter of $\tilde{A}(\nu)$ (0.25 μm^{-1}) takes 78% of the lateral bandwidth of the detector (0.32 μm^{-1}), making it impossible to avoid the spectral overlap.

The SBP of the proposed method can be further improved by introducing anamorphic imaging. The bandwidth required for the proposed method in the direction perpendicular to the modulation is half the bandwidth required in the modulation direction (see Supplement 1 for details). By magnifying the image differently in x and y directions, the SBP can be further increased. As a proof of concept, wide FoV imaging in the anamorphic condition is demonstrated. First, the experimental setup is modified as in Fig. S2(b). The anamorphic imaging is achieved with two sets of 4-f telescopic imaging arrays using cylindrical lenses. The same objective lens as in the case of human breast tissue is adopted. The total magnification of the setup is 8.333 and 4.166 in x and y directions, respectively. Mouse brain tissue, prepared according to the protocol in [38], is imaged. The aberration induced by the cylindrical lenses has been numerically compensated (see Supplement 1).

The measured quantitative phase image is shown in Fig. 4. We found a diagonal fringe in the phase originating from the surface reflection between two coverslips, due to variation in optical thickness across the wide FoV [Fig. 4(a)]. This artifact is suppressed with the assumption that the sample does not exhibit a structure larger than 100 μm (details in Supplement 1).

The corrected image is shown in Fig. 4(b). The FoV of the images is 1.58 × 2.11 mm with a diffraction-limited size of 0.96 μm. The SBP of the measured complex amplitude image is 4.2 megapixels. Figure 4(c) shows the Fourier spectrum of

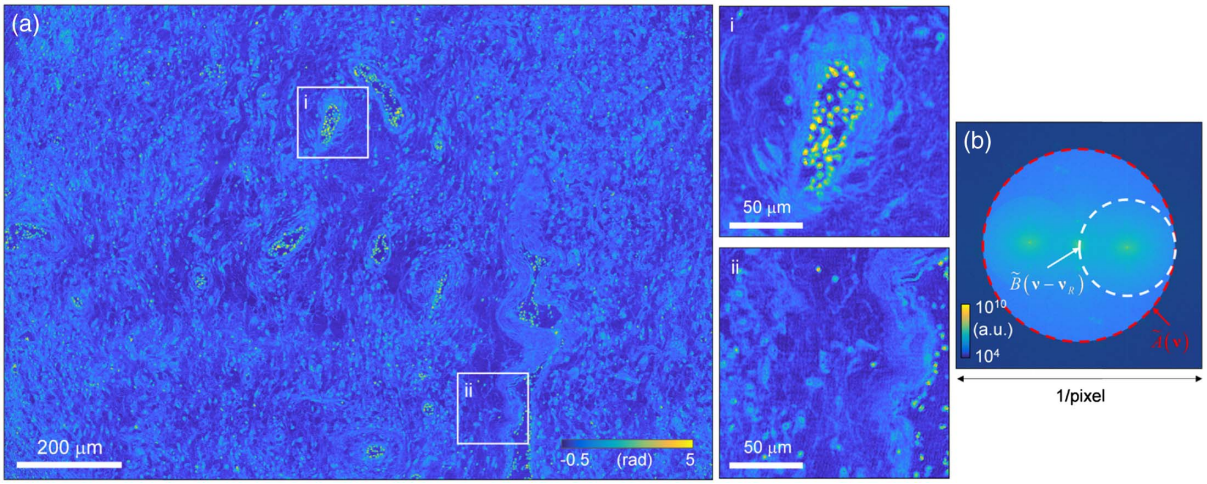

Fig. 3. Experimental demonstration of wide field of view quantitative phase imaging. (a) Measured quantitative phase image of breast tissue with the proposed method. Insets show magnified images at different positions. (b) Fourier spectrum of an interferogram.

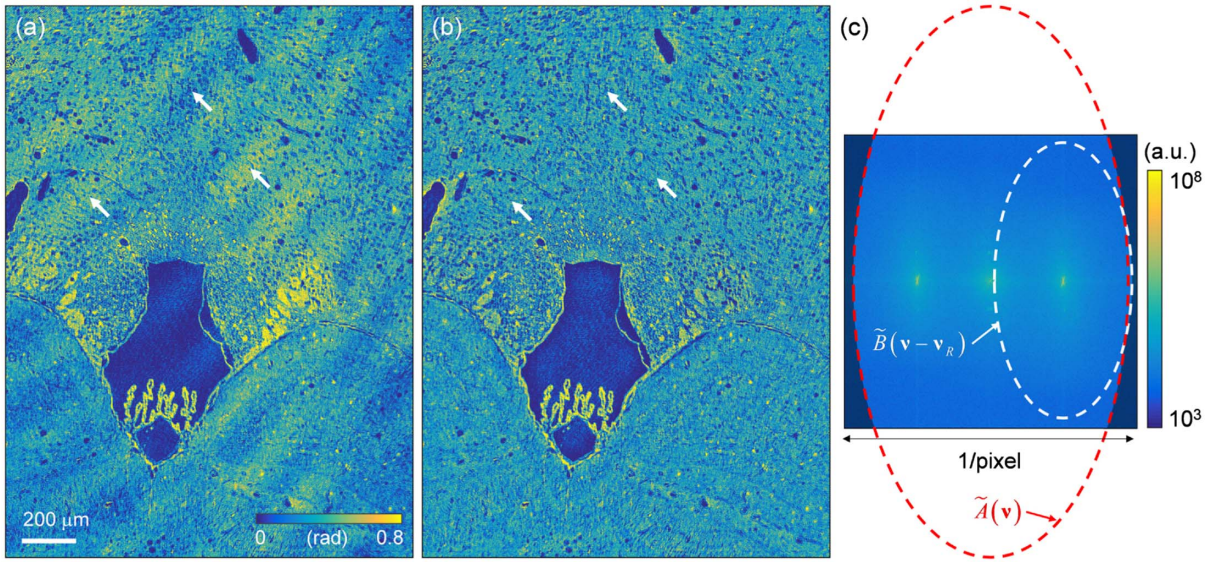

Fig. 4. Experimental demonstration with anamorphic imaging. (a) Quantitative phase image of mouse brain tissue retrieved using the proposed method. (b) Corrected image of (a), where the multiple reflections induced by coverslips are removed (indicated with white arrows). (c) Fourier spectrum of an interferogram.

the off-axis interferogram. The term $\tilde{B}(\nu-\nu_R)$ completely occupies the vertical bandwidth of the detector, and $\tilde{A}(\nu)$ exceeds the bandwidth of the detector. Consequently, the conventional off-axis method suffers from spectral overlap (see Supplement 1). In addition, bright-field microscopy will not be free from aliasing at this imaging condition. In Fig. 4, however, bright-field microscopy is unsuitable because the sample is a 3-μm-thick unstained brain tissue slice. Thus, the sample is highly transparent, which can be visualized with quantitative phase images, not with intensity images. On the contrary, the proposed method enables correct retrieval of a complex amplitude image. Furthermore, the bright-field counterpart of the measured complex amplitude image has an SBP of 16.7 megapixels. Considering that the SBP of the detector is 12 megapixels, the amount of information measured in the proposed method exceeds not only that of the conventional off-axis method, but also that of bright-field microscopy. In Fig. 5, the SBPs per measurement of various methods are shown as a function of the pixel count of a detector. It is assumed that the pixel count of a detector becomes a bottleneck to SBPs. Each line indicates the maximum available SBP per measurement for a given detector pixel count. Thus experimental values lie below their corresponding lines. Iterative high-SBP techniques [5] exhibit relatively low SBP per measurement because of data redundancy and multiple measurements. Instead, they take advantage of simple setups without the need of interferometry. Data points of references are calculated using the following values. For out-of-focusing imaging pixel super-resolution (OFI-PSR) [7], 4.6 mm^2 FoV, 0.3 NA at 532 nm, five images, and the pixel count of 1.45 million are used. For Fourier ptychography [5], 120 mm^2 FoV, 0.5 NA at 632 nm, 137 images, and the pixel

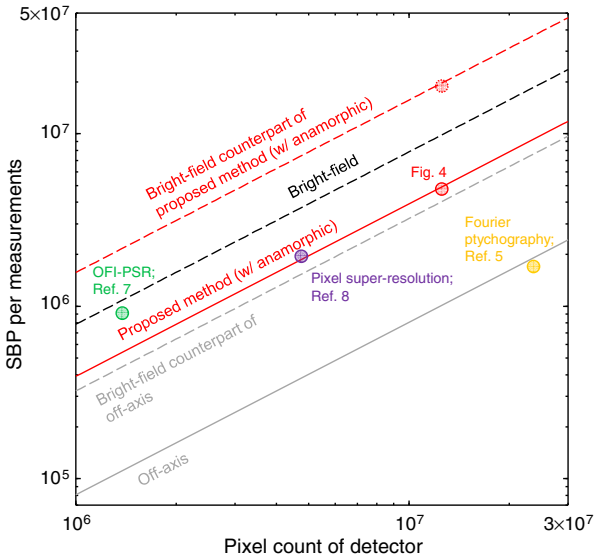

Fig. 5. SBP per measurements and pixel count of detectors achieved in different works. Solid and dashed lines indicate the maximum achievable SBP per measurements of complex amplitude and intensity images, respectively, in different imaging techniques. The proposed method achieves a 4.2-megapixel complex amplitude image with a 12-megapixel detector (red circle, data shown in Fig. 4). The bright-field counterpart of the measured complex amplitude image has an SBP of 16.7 megapixels (dashed red circle). Achieved SBP per measurements and pixel count of detectors in the literatures (Refs. [5,7,8]) are denoted with colored circles.

count of 23 million are used. For pixel super-resolution, 24 mm^2 FoV, 0.5 NA at 500 nm, 36 images, and the pixel count of five million.

4. DISCUSSION AND CONCLUSION

We have demonstrated a method for high-SBP off-axis holographic imaging. Exploiting the KK relations, the proposed method retrieves an exact complex amplitude without imposing any constraint on a sample. It efficiently utilizes the interferogram bandwidth to provide a 3.34- to 4-fold increase in the SBP compared to the conventional method. Furthermore, with anamorphic imaging, the bright-field counterpart of the measured complex amplitude exhibits an SBP greater than the SBP of the detector.

The proposed method is fundamentally different from previous methods for zero-order suppression under the spectral overlap in off-axis geometry. The proposed method requires a single interferogram. This is in contrast to the previous method, where multiple interferograms are required [20,21,24,39,40]. In addition, the proposed method provides an analytic expression for the complex amplitude without imposing a constraint on a sample. Thus, the retrieval process is simple, and the measured complex amplitude is exact. Existing methods require assumptions for a sample, such as uniform intensity [22,26], weak phase [23,41], weak phase gradient [25], or slowly varying complex amplitude [27,42], to guarantee correct measurement of complex amplitudes.

Despite similarities with the nonlinear filtering method [29], the proposed method does not require a complex amplitude image to be confined within a quadrant of the frequency space. On the other hand, the proposed method requires the analyticity condition of the KK relations, which allows a reduced interferogram bandwidth that is less than that demonstrated in the previous study. Importantly, the proposed method does not require a bandwidth that is more than the size of a pupil function in the direction perpendicular to modulation. This feature enables a further enhanced SBP by adopting anamorphic imaging. Also, by generalizing the principle to three dimensions, e.g., using $\chi(x, y, \nu_z)$ and its analyticity in UHP of ν_z, the proposed method can provide a framework that can embrace the different principles for off-axis [29] and on-axis [43] configurations. The proposed method requires an image of the reference beam in addition to an off-axis interferogram. Nevertheless, the image of the reference beam needs to be measured once. Thus, the proposed method effectively becomes a single-shot method with a stable setup. This becomes particularly useful for large FoV image stitching or time-lapse imaging, where a large number of images are used. It should also be noted that the proposed method is available with spatially coherent light.

The proposed method can be combined with other techniques, such as synthetic aperture microscopy [44], optical diffraction tomography [45–47], and common-path off-axis interferometers [48–50]. We envision that the proposed method will benefit holographic imaging with an enhanced SBP and become an effective tool for 3D imaging, high-throughput histopathology, and large-scale studies of cells and tissue.

Funding. National Research Foundation of Korea (NRF) (2015R1A3A2066550, 2017M3C1A3013923, 2018K000396, 2018R1A6A3A01011043); KAIST; Tomocube; BK21+ program.

Acknowledgment. We thank Seonggeun Kim for the helpful discussion. We also thank Lunit Inc. for providing the breast tissue slide.

See Supplement 1 for supporting content.

REFERENCES

1. A. W. Lohmann, R. G. Dorsch, D. Mendlovic, Z. Zalevsky, and C. Ferreira, "Space-bandwidth product of optical signals and systems," J. Opt. Soc. Am. A **13**, 470–473 (1996).
2. F. Ghaznavi, A. Evans, A. Madabhushi, and M. Feldman, "Digital imaging in pathology: whole-slide imaging and beyond," Annu. Rev. Pathol. **8**, 331–359 (2013).
3. P. Lang, K. Yeow, A. Nichols, and A. Scheer, "Cellular imaging in drug discovery," Nat. Rev. Drug. Discov. **5**, 343–356 (2006).
4. V. C. Abraham, D. L. Taylor, and J. R. Haskins, "High content screening applied to large-scale cell biology," Trends Biotechnol. **22**, 15–22 (2004).
5. G. Zheng, R. Horstmeyer, and C. Yang, "Wide-field, high-resolution Fourier ptychographic microscopy," Nat. Photonics **7**, 739–745 (2013).
6. S. Dong, R. Horstmeyer, R. Shiradkar, K. Guo, X. Ou, Z. Bian, H. Xin, and G. Zheng, "Aperture-scanning Fourier ptychography for 3D refocusing and super-resolution macroscopic imaging," Opt. Express **22**, 13586–13599 (2014).
7. H. Wang, Z. Göröcs, W. Luo, Y. Zhang, Y. Rivenson, L. A. Bentolila, and A. Ozcan, "Computational out-of-focus imaging increases the space-bandwidth product in lens-based coherent microscopy," Optica **3**, 1422–1429 (2016).
8. W. Bishara, T. W. Su, A. F. Coskun, and A. Ozcan, "Lensfree on-chip microscopy over a wide field-of-view using pixel super-resolution," Opt. Express **18**, 11181–11191 (2010).
9. J. R. Carson, "Method and means for signaling with high-frequency waves," U.S. patent application US1449382A (March 27, 1923).

10. G. T. Di Francia, "Degrees of freedom of an image," J. Opt. Soc. Am. **59**, 799–804 (1969).
11. M. K. Kim, "Principles and techniques of digital holographic microscopy," Proc. SPIE **1**, 018005 (2010).
12. K. Lee, K. Kim, J. Jung, J. Heo, S. Cho, S. Lee, G. Chang, Y. Jo, H. Park, and Y. Park, "Quantitative phase imaging techniques for the study of cell pathophysiology: from principles to applications," Sensors **13**, 4170–4191 (2013).
13. Y. Park, C. Depeursinge, and G. Popescu, "Quantitative phase imaging in biomedicine," Nat. Photonics **12**, 578–589 (2018).
14. M. Takeda, H. Ina, and S. Kobayashi, "Fourier-transform method of fringe-pattern analysis for computer-based topography and interferometry," J. Opt. Soc. Am. **72**, 156–160 (1982).
15. E. Cuche, P. Marquet, and C. Depeursinge, "Simultaneous amplitude-contrast and quantitative phase-contrast microscopy by numerical reconstruction of Fresnel off-axis holograms," Appl. Opt. **38**, 6994–7001 (1999).
16. A. Lohmann, "Reconstruction of vectorial wavefronts," Appl. Opt. **4**, 1667–1668 (1965).
17. J. Kuhn, T. Colomb, F. Montfort, F. Charriere, Y. Emery, E. Cuche, P. Marquet, and C. Depeursinge, "Real-time dual-wavelength digital holographic microscopy with a single hologram acquisition," Opt. Express **15**, 7231–7242 (2007).
18. C. Yuan, H. Zhai, and H. Liu, "Angular multiplexing in pulsed digital holography for aperture synthesis," Opt. Lett. **33**, 2356–2358 (2008).
19. T. Tahara, Y. Takahashi, and Y. Arai, "Image-quality improvement in space-bandwidth capacity-enhanced digital holography," Opt. Eng. **53**, 112313 (2014).
20. Y. Takaki, H. Kawai, and H. Ohzu, "Hybrid holographic microscopy free of conjugate and zero-order images," Appl. Opt. **38**, 4990–4996 (1999).
21. Y. M. Zhang, Q. N. Lu, and B. Z. Ge, "Elimination of zero-order diffraction in digital off-axis holography," Opt. Commun. **240**, 261–267 (2004).
22. T. M. Kreis and W. P. O. Juptner, "Suppression of the DC term in digital holography," Opt. Eng. **36**, 2357–2360 (1997).
23. G. L. Chen, C. Y. Lin, M. K. Kuo, and C. C. Chang, "Numerical suppression of zero-order image in digital holography," Opt. Express **15**, 8851–8856 (2007).
24. N. Demoli, J. Mestrovic, and I. Sovic, "Subtraction digital holography," Appl. Opt. **42**, 798–804 (2003).
25. J. Weng, J. Zhong, and C. Hu, "Digital reconstruction based on angular spectrum diffraction with the ridge of wavelet transform in holographic phase-contrast microscopy," Opt. Express **16**, 21971–21981 (2008).
26. T. Ikeda, G. Popescu, R. R. Dasari, and M. S. Feld, "Hilbert phase microscopy for investigating fast dynamics in transparent systems," Opt. Lett. **30**, 1165–1167 (2005).
27. K. Khare, P. T. Ali, and J. Joseph, "Single shot high resolution digital holography," Opt. Express **21**, 2581–2591 (2013).
28. M. Liebling, T. Blu, and M. A. Unser, "Non-linear Fresnelet approximation for interference term suppression in digital holography," Proc. SPIE **5207**, 553–560 (2003).
29. N. Pavillon, C. S. Seelamantula, J. Kuhn, M. Unser, and C. Depeursinge, "Suppression of the zero-order term in off-axis digital holography through nonlinear filtering," Appl. Opt. **48**, H186–H195 (2009).
30. N. Pavillon, C. Arfire, I. Bergoend, and C. Depeursinge, "Iterative method for zero-order suppression in off-axis digital holography," Opt. Express **18**, 15318–15331 (2010).
31. M. Liebling, T. Blu, and M. Unser, "Complex-wave retrieval from a single off-axis hologram," J. Opt. Soc. Am. A **21**, 367–377 (2004).
32. E. Sanchez-Ortiga, A. Doblas, G. Saavedra, M. Martinez-Corral, and J. Garcia-Sucerquia, "Off-axis digital holographic microscopy: practical design parameters for operating at diffraction limit," Appl. Opt. **53**, 2058–2066 (2014).
33. R. D. L. Kronig, "On the theory of dispersion of x-rays," J. Opt. Soc. Am. **12**, 547–557 (1926).
34. H. A. Kramers, "La diffusion de la lumière par les atomes," in *Atti Cong. Intern. Fisici, (Transactions of Volta Centenary Congress) Como.* (1927), Vol. **2**, pp. 545–557.
35. A. Mecozzi, C. Antonelli, and M. Shtaif, "Kramers-Kronig coherent receiver," Optica **3**, 1220–1227 (2016).
36. H. Voelcker, "Demodulation of single-sideband signals via envelope detection," IEEE Trans. Commun. Technol. **14**, 22–30 (1966).
37. E. C. Titchmarsh, *Introduction to the Theory of Fourier Integrals* (Clarendon, 1948), Vol. **2**.
38. M. Lee, E. Lee, J. Jung, H. Yu, K. Kim, J. Yoon, S. Lee, Y. Jeong, and Y. Park, "Label-free optical quantification of structural alterations in Alzheimer's disease," Sci. Rep. **6**, 31034 (2016).
39. N. T. Shaked, Y. Zhu, M. T. Rinehart, and A. Wax, "Two-step-only phase-shifting interferometry with optimized detector bandwidth for microscopy of live cells," Opt. Express **17**, 15585–15591 (2009).
40. M. G. Shan, M. E. Kandel, H. Majeed, V. Nastasa, and G. Popescu, "White-light diffraction phase microscopy at doubled space-bandwidth product," Opt. Express **24**, 29033–29039 (2016).
41. L. Xue, J. Lai, S. Wang, and Z. Li, "Single-shot slightly-off-axis interferometry based Hilbert phase microscopy of red blood cells," Biomed. Opt. Express **2**, 987–995 (2011).
42. D. Kim, R. Magnusson, M. Jin, J. Lee, and W. Chegal, "Complex object wave direct extraction method in off-axis digital holography," Opt. Express **21**, 3658–3668 (2013).
43. Y. Zhang, G. Pedrini, W. Osten, and H. J. Tiziani, "Reconstruction of in-line digital holograms from two intensity measurements," Opt. Lett. **29**, 1787–1789 (2004).
44. F. Le Clerc, M. Gross, and L. Collot, "Synthetic-aperture experiment in the visible with on-axis digital heterodyne holography," Opt. Lett. **26**, 1550–1552 (2001).
45. Y. Cotte, F. Toy, P. Jourdain, N. Pavillon, D. Boss, P. Magistretti, P. Marquet, and C. Depeursinge, "Marker-free phase nanoscopy," Nat. Photonics **7**, 113–117 (2013).
46. K. Kim, J. Yoon, S. Shin, S. Lee, S.-A. Yang, and Y. Park, "Optical diffraction tomography techniques for the study of cell pathophysiology," J. Biomed. Photon. Eng. **2**, 020201 (2016).
47. E. Wolf, "Three-dimensional structure determination of semi-transparent objects from holographic data," Opt. Commun. **1**, 153–156 (1969).
48. G. Popescu, T. Ikeda, R. R. Dasari, and M. S. Feld, "Diffraction phase microscopy for quantifying cell structure and dynamics," Opt. Lett. **31**, 775–777 (2006).
49. B. Bhaduri, H. Pham, M. Mir, and G. Popescu, "Diffraction phase microscopy with white light," Opt. Lett. **37**, 1094–1096 (2012).
50. K. Lee and Y. Park, "Quantitative phase imaging unit," Opt. Lett. **39**, 3630–3633 (2014).